Hindawi
Journal of Engineering
Volume 2022, Article ID 7555127, 11 pages
https://doi.org/10.1155/2022/7555127

*Research Article*

# Behavior of Multispan Extradosed Bridge Subjected to Variation of Cable-Free Segment Length

**Lifeng Wang**,[1] **Saisai Yu**,[1] **Long Liu**,[1,2] **and Ziwang Xiao**[1]

[1]*Northeast Forestry University, Harbin, China*
[2]*Anyang Institute of Technology, Anyang, China*

Correspondence should be addressed to Lifeng Wang; lifengwang@nefu.edu.cn

Received 18 July 2021; Accepted 8 February 2022; Published 28 February 2022

Academic Editor: Francesco Tornabene



Based on the main bridge of the Paira Bridge in Bangladesh, this paper studies the behavior of multispan extradosed bridge subjected to variation of cable-free segment length. First, a finite element simulation model was established, and linear analysis was performed. The accuracy of the finite element model was verified by comparing the measured data with the finite element analysis. Then the influences of the cable-free segment length in the midspan and the pylon root on the horizontal displacement of the pylon top, the vertical deflection of the midspan, and the bending moment of the main girder were analyzed, respectively. The results showed that the variation of the cable-free segment length put a significant impact on the horizontal displacement of the pylon top and the vertical displacement of the middle of each span. The increase of positive moment was greater than negative moment when the cable-free segment length in the middle of the span increased. However, when the cable-free segment length of the pylon root increased, the negative bending moment of the main girder increased more than the positive bending moment.

## 1. Introduction

The extradosed bridge is a structural system interposed between the continuous girder bridge and cable-stayed bridge [1, 2]. Based on the difference of stiffness between the main girder and the pylons, the extradosed bridge can be divided into rigid girder extradosed bridge and flexible girder extradosed bridge [3]. At this stage, most of the rigid girder extradosed bridges built domestically and abroad are characterized by greater stiffness of the main girder and lower stiffness of the bridge pylon, and the cable-free segment is located at the root of the pylon and midspan of the main girder (in Figure 1(a), $L_1$ is the length of the cable-free segment in the middle of span; $L_2$ is the length of the cable-free segment at the root of the pylon).

It was proved that the length variation of cable-free segment of cable-stayed bridges has different effects on structural characteristic parameters [4–6]. In this area, many scholars have done research. Liu Wenhui and others took the bending moment of the main girder of the cable-stayed bridge with two pylons as the control target [7] and changed the distribution of stay cables. It was concluded that when the ratio of the length of the cable-free segment at the root of the bridge pylon to the span of the main girder was 0.13 and the ratio of the length of the cable-free segment of the midspan to the span of the main girder was 0.25, the bending moment distribution of the main girder was more reasonable. Zhou Zijie and others analyzed the influence of the length of cable-free segment of the single-pylon cable-stayed bridge with hybrid girder on the deflection of the main girder through the qualitative of equivalent beams and found that the optimum value was when the cable-free length was 0.2 times the length of midspan [8]. By studying the length variation of cable-free segment at the root of the pylon of the cable-stayed bridge with two pylons, Li Zhen [9] found that the main girder displacement was small when the ratio of length of cable-free segment to length of midspan was 0.175–0.219. Based on the analysis of the influence of structural design parameters on the internal force and displacement of the main girder of the extradosed bridge with high piers and two pylons, Zhang Xinjun and others concluded that when the length of cable-free segment at the

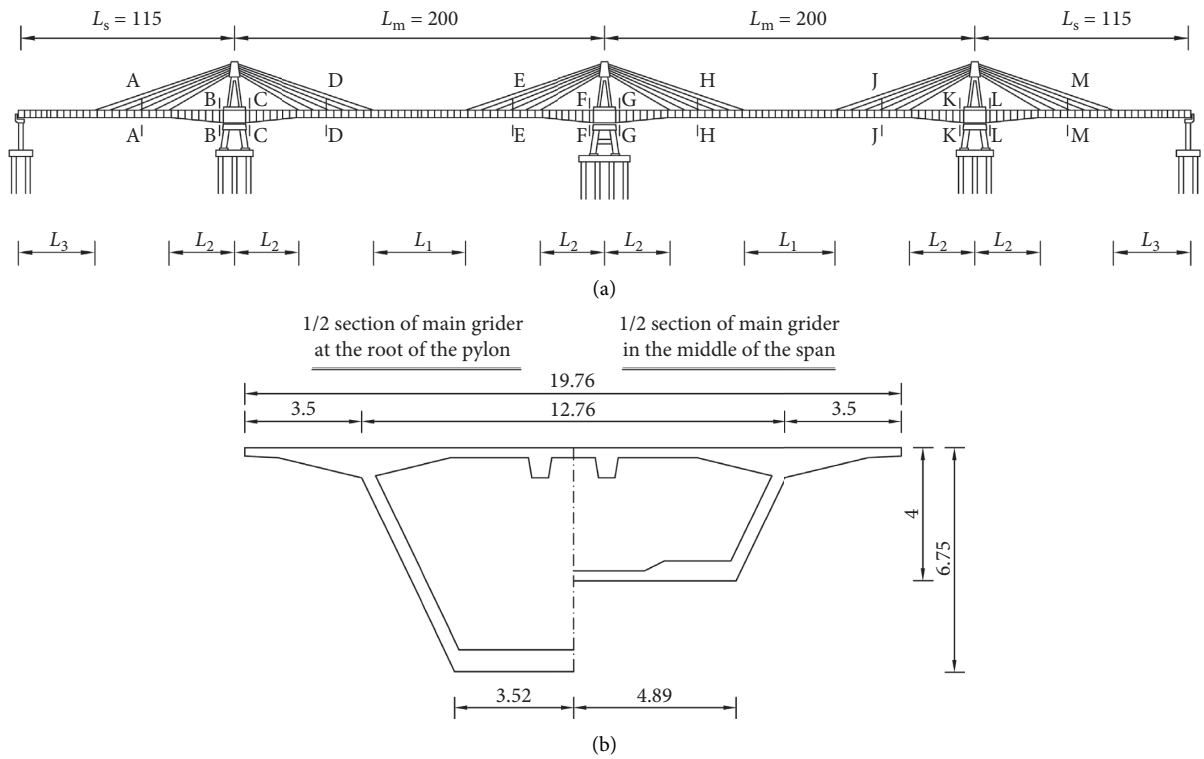


Figure 1: The layout and standard cross section of the main bridge of Paira Bridge in Bangladesh. (a) Layout of the bridge type (unit: m). (b) Standard cross-sectional arrangement (unit: m).

root of the pylon and the length of cable-free segment in the middle of the span were smaller, the main girder bore reasonable force and the displacement was small [10].

Luo Chengbin et al. investigated the influence of the longitudinal displacement of the pylon on the main girder alignment, cable force, the stress of the pylon, and the stress of the main girder and concluded that the longitudinal deflection of the bridge pylon has a greater influence on the stress of the bridge pylon than the effect on the main girder stress [11]. Bin Wang et al. coupled wind load-bridge-car load to the car to analyze the safety of the car [12]. They concluded that the bridge pylon has a greater impact on the rolling and lateral movement of vehicles. It can be seen from the above literature that the deflection of the bridge pylon has a greater impact on the stress of the bridge pylon. In a multispan extradosed bridge, there are no end anchor cables and auxiliary piers at both ends of the middle pylon to limit the structural deformation, resulting in lower overall stiffness of the bridge. Under live loading, the deflection of the main girder in the span and the deflection of the bridge pylon are significant [13–15]. Scholars at home and abroad have done more research on the deflection of the main girder, but less on the deflection of the bridge pylon. Zhang Ning et al. analyzed the influence of the pylon's sunshine temperature effect on the deflection of the H-shaped concrete bridge pylon [16]. The study showed that the maximum pylon deviation exceeded 40 mm in one day in winter, which was not conducive to monitor the pylon deviation during construction. Under the background of special-shaped cable-stayed bridge, Liu Zengwu et al. studied the influence of different parameters on the stress and deviation of cable pylon [17]. The study found that the weight of the girder and shrinkage and creep had a greater impact on the displacement of the bridge pylon.

Previous scholars have done a lot of research on the influence of length variation in the cable-free segment on the static and dynamic performance of single-pylon and two-pylon cable-stayed bridges [18, 19]. At present, there are few studies on the influence of length variation on the structural behavior of cable-free segment of cable-stayed bridge with three pylons and above. Their research on the ratio of the length of the cable-free segment to the length of the midspan rarely covers the range recommended by the "Specifications for Design of Highway Cable-stayed Bridge" (hereinafter referred to as the "specifications") [20]. Because the multispan extradosed bridge is a superstationary structure, the influence of the length variation of the cable-free segment on the horizontal displacement of the top of the pylon and the vertical deflection in the span is complicated. Therefore, based on the main bridge of Paira Bridge in Bangladesh, by changing the length of cable-free segment between the middle of span and the root of pylon, this paper studies the variation rule of structural behavior within the range of the ratio of the cable-free segment length to the midspan length recommended by the specifications, which is expected to provide a basis for the design of the same type of bridge.

## 2. Establishment of the Analysis Model

*2.1. Engineering Background.* The Paira Bridge in Bangladesh is located in the Barisal District of Bangladesh and is used as a bridge connecting Barisal and PATUAKHALI. Northeast Forestry University is the construction monitoring unit for the bridge. The main bridge of the Paira Bridge is a cable-stayed bridge with three pylons and four spans, and its span combination is (115 + 2×200 + 115) *m*. It adopts a rigid frame system. The bridge layout and standard cross-section are shown in Figure 1. The bridge pylon is constructed of reinforced concrete with a height of 25.8 m and made of C60 high-strength concrete. Last but not least, the stay cable is composed of 91 low-relaxation 1860 steel strands with a diameter denoted with Φ equal to 15.2 mm. There are 6 stay cables on each side of a pylon, and the distance between stay cables is 8m. The main girder is made of C60 high-strength concrete, and its section is a single-box single-chamber box girder with variable height. The width of the top plate is 19.76 m; the cantilever length of the flange is 3.5 m; the thickness of the web is 0.4 m; the width of the bottom plate is (7.039 ~ 9.787) *m*, and its thickness is (0.30 ~ 0.65) *m*. The height of the girder at the support is 6.75 m; the height of the girder at the middle of span is 4.00 m, and change of the height of forms for the quadratic parabola. The length of the cable-free segment in the middle of the main girder ($L_1$) is 49.5 mm; the length of the cable-free segment at the root of the pylon ($L_2$) is 35.25 m, and the length of the cable-free segment at the end of the side pylon ($L_3$) is 41.1 m. The length of the corresponding cable-free segment is indicated in Figure 1(a). Figure 2 shows real view and completion of the main bridge of Paira Bridge in Bangladesh.

*2.2. Finite Element Analysis Model.* To analyze the influence of the ratio of length of cable-free segment to length of midspan of the three-pylon extradosed bridge on structural behavior of the structure, MIDAS/CIVIL 2020 was used to establish the finite element analysis model. Among them, piers, girder, and bridge pylons were all simulated by girder elements, and stay cables were simulated by truss elements. Elastic modulus and capacity of concrete are measured by the test, concrete compressive curve reference [21] and concrete shrinkage creep curve reference [22]. The bottom of the pier was restrained by fixed ends; the bridge pylon and the girder were rigidly connected; and the pier and the girder were rigidly connected. Simple support constraints were adopted at the cast in situ section of the girder side span. The bridge has a total of 291 nodes and 312 elements, of which 36 are cable-stayed elements, 208 are girder elements, 42 are pylon elements, and 26 are pier elements. Linear analysis is used for model calculations. The loads are vertical, static vehicle loads, which are arranged according to the influence line at locations that make certain sections of the structure most unfavorable. The finite element model of the full bridge is shown in Figure 3.

## 3. Finite Element Verification

To ensure the accuracy of the finite element model for the parametric analysis below, the finite element model results are compared with the measured data. The location of the measurement points on site is shown in Figure 4, where 1–5 are stress measurement points and A ~ E are elevation measurement points.

*3.1. Deformation Analysis.* This paper analyzes the theoretical and measured elevations of the top plate in two representative states: the maximum cantilever state of the middle pier and the completion state of the bridge (the measured elevation is the average of the elevation of three measurement points on the top plate). The comparative data are shown in Figure 5. To clearly show the specific differences between the measured and theoretical elevations, the relative elevation difference (measured elevation-theoretical elevation) is given in Figure 6.

As can be seen from Figures 5 and 6, the measured elevation of the main girder is not significantly different within $L_m/4$ from the bridge pylon at the maximum cantilever condition, and the measured elevation from $L_m/4$ to $L_m/2$ first drops and then rises. The maximum measured elevation is 27.675 m and the minimum measured elevation is 27.068 m. The maximum error between the theoretical elevation and the measured elevation is 9.5 mm, which occurs at the outermost end of the cantilever. After the completion of the bridge, the maximum measured elevation appears in the middle pylon and gradually drops to both sides. The maximum measured elevation is 27.665 m and the maximum theoretical elevation is 27.659 m. The maximum error between the theoretical elevation and the measured elevation is 10.4 mm, which occurs at the position of $L_m/6$ from the left pylon. Under the two conditions, the variation trend of the theoretical elevation is consistent with that of the measured elevation, and the error is small, indicating that the finite element model is in good agreement with the actual construction.

*3.2. Stress Analysis.* The location of the main beam stress monitoring arrangement is shown in Figure 1. It sets up 12 stress monitoring sections. Each section top plate set three measurement points, and bottom plate set two measurement points (the measured stress of the top plate is taken as the average of three points, and the bottom plate is taken as the average of two points). The measured stress of the top and bottom plates of sections B, C, and F at different construction stages is compared with the theoretical stress, as shown in Figure 7.

As can be seen from Figure 7, the compressive stress in the top plate of each section shows an overall trend of first increasing and then decreasing as the construction progresses. Local stress mutation occurs due to cable tension. The maximum measured compressive stress in section B is 20.87 MPa and the maximum theoretical compressive stress

(a) (b)

Figure 2: Real view and completion of the main bridge of Paira Bridge in Bangladesh. (a) Real view of the construction site. (b) Real view of completion of the main bridge.

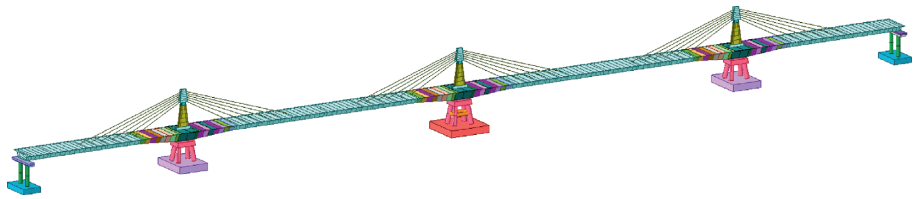

Figure 3: Finite element model of the full bridge.

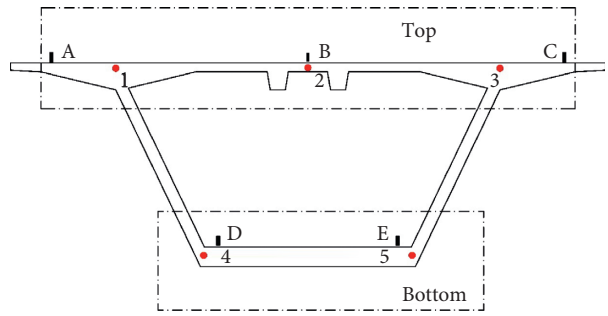


Figure 4: Measuring points.

is 20.80 MPa, with the maximum error of 1.17 MPa, which occurs in stage 59. The maximum measured compressive stress in section C is 21.34 MPa, and the maximum theoretical compressive stress is 21.00 MPa. The maximum measured compressive stress in section F is 21.63 MPa and the maximum theoretical compressive stress is 21.00 MPa, with the maximum error of 1.36 MPa, which occurs in stage 47. The bottom plate is initially compressive stress and gradually increases. With the tension of the cable and the concrete pouring, the bottom plate stress transforms between tensile stress and compressive stress and finally settled at the compressive stress, and the compressive stress gradually increases in the later period. The maximum measured tensile stress in section B is 2.11 MPa and the maximum theoretical tensile stress is 1.94 MPa. The maximum measured tensile stress in section C is 2.13 MPa and the maximum theoretical tensile stress is 1.98 MPa. The maximum measured tensile stress in section F is 2.13 MPa and the maximum theoretical tensile stress is 1.96 MPa. The maximum tensile stress in the bottom plate all appears in the 51st stage (second tensioning of the outermost cable). During the construction stage, the measured stress and calculated stress in each section have the same trend. The difference between the two numbers is small, and the error is within 10% of each other.

The above analysis shows that the finite element model results are consistent with the measured data within the error range allowed by the project. This shows the accuracy of the calculation model and ensures the reliability of the analysis results in the following chapter.

## 4. Influence of Length Variation of the Cable-Free Segment on Structural Behavior

On the basis of the original design parameters, the distance between cables, the cross-sectional area of cables, the number of cables, the height of pylons, and the stiffness of pylons remain unchanged. The midspan change of the main girder will inevitably cause the change of the ratio of the length of the cable-free segment to the midspan length. The specific

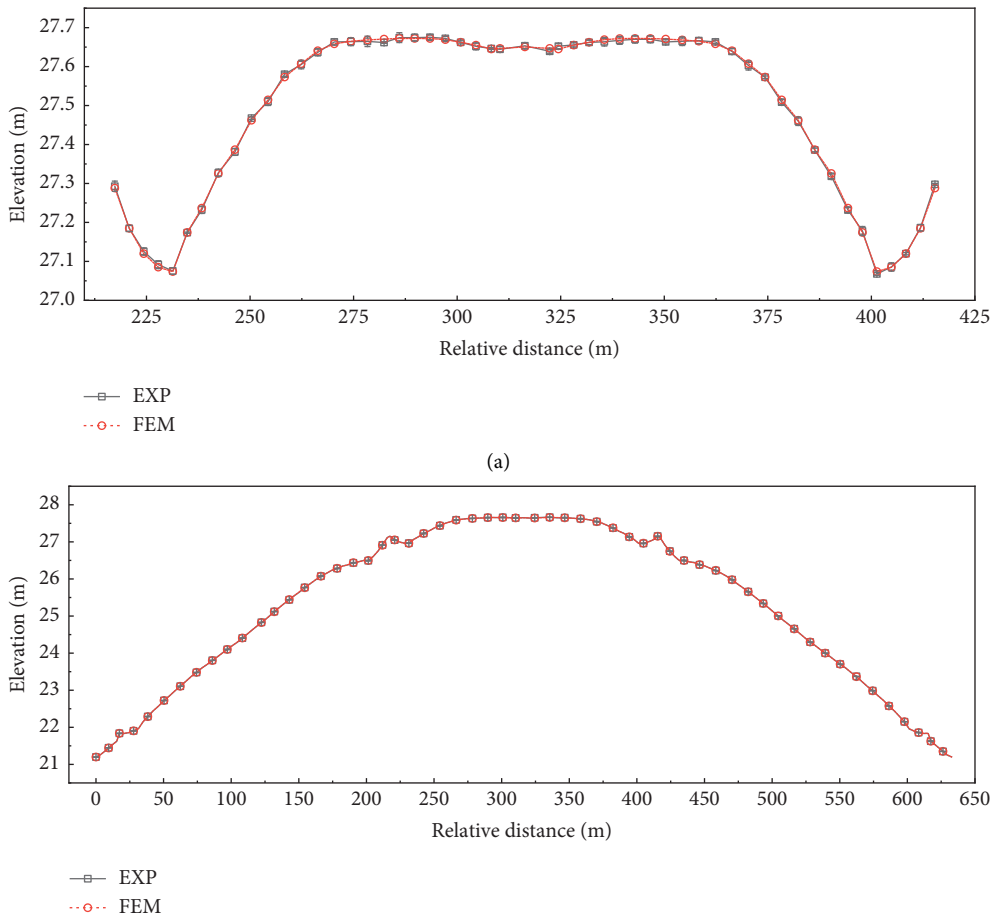


Figure 5: Comparison of measured elevation and theoretical elevation. (a) Maximum cantilever state of the middle pier. (b) Bridge completion.

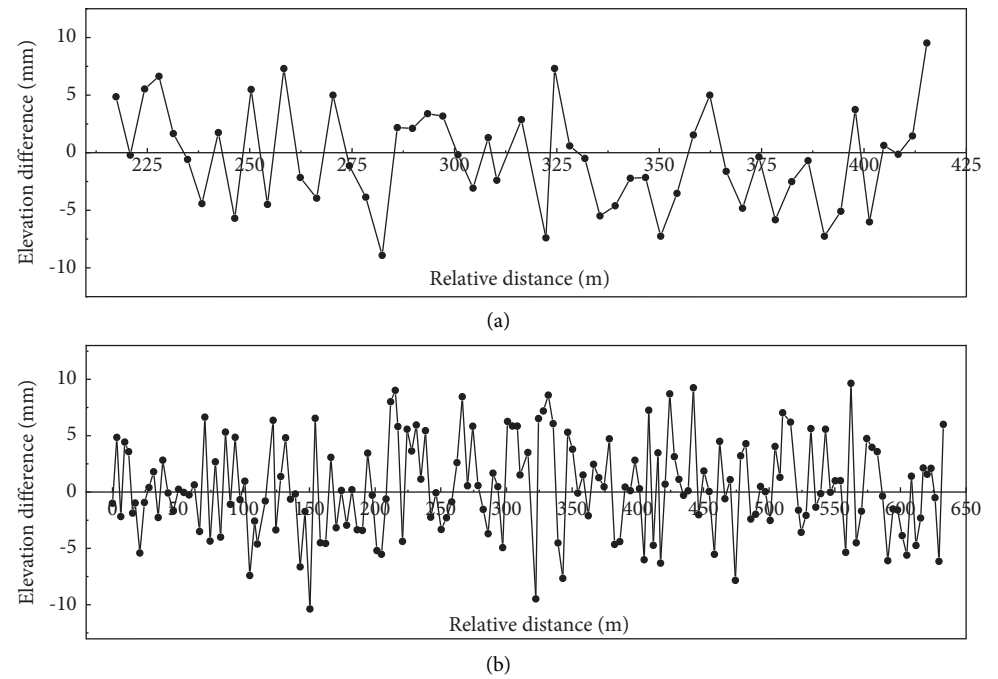


Figure 6: Difference between measured elevation and theoretical elevation. (a) Maximum cantilever state of the middle pier. (b) Bridge completion.

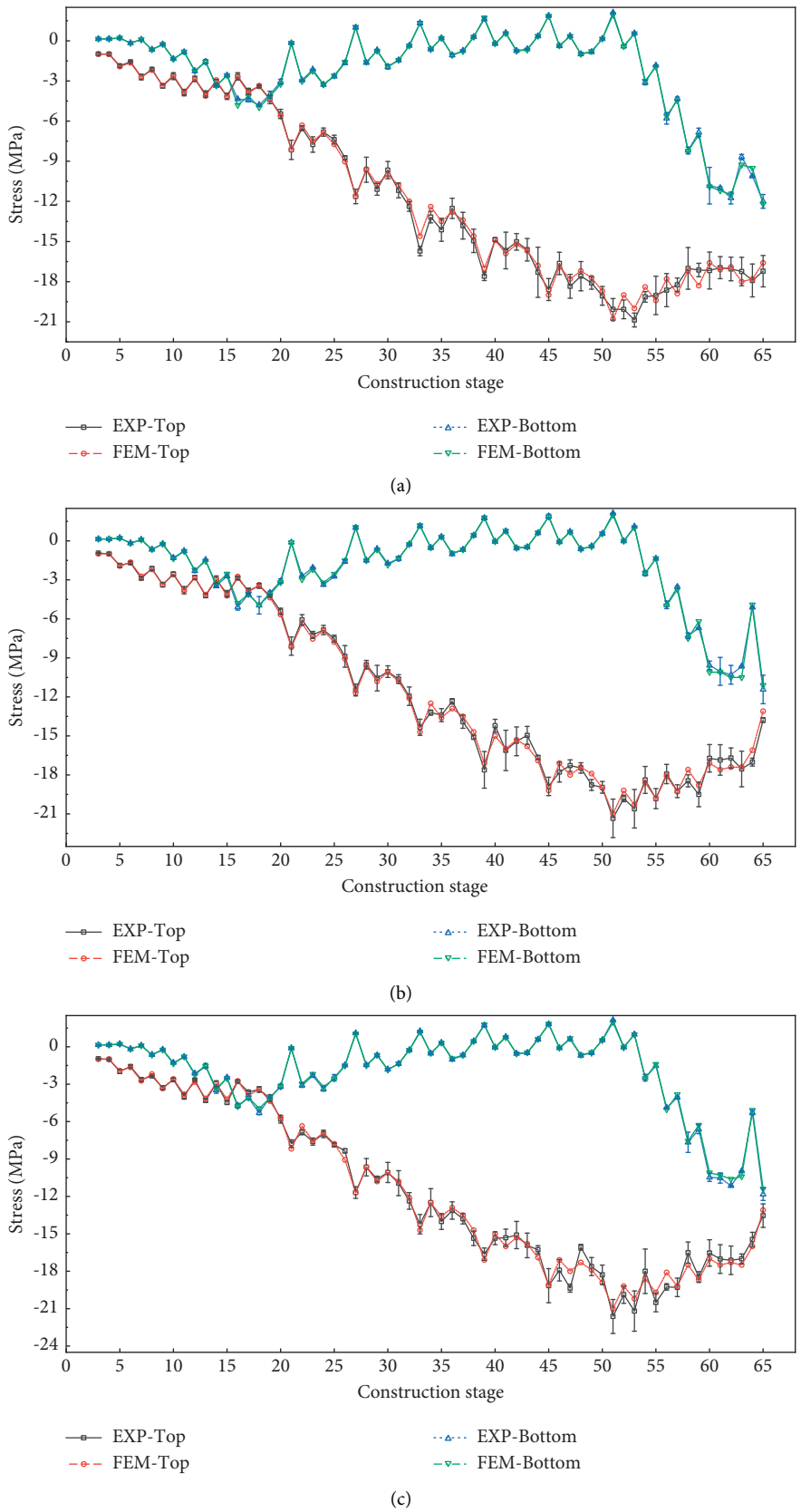


Figure 7: Comparison of measured stress and theoretical stress. (a) B-B section stress. (b) C-C section stress. (c) F-F section stress.

implementation method is as follows: on the basis of 160m, the midspan length of the girder was increased every 10m to 240m to analyze the effect of the increase in the ratio of the length of the cable-free segment to the length of midspan on the horizontal displacement of the three-pylon cable-stayed bridge, the deflection of the main girder, and the bending moment. In order to make the research content more universal, define the ratio $\lambda$ of the cable-free segment as follows:

$$\lambda = \frac{L}{L_m}, \tag{1}$$

where $L$ is the length of cable-free segment and $L_{\mathrm{m}}$ is the length of midspan.

Figure 8 shows the change in the ratio of the cable-free segment in the middle of the span ($\lambda_1$) and the ratio of the cable-free segment at the root of pylon ($\lambda_1$).

*4.1. Influence of Length Variation of the Cable-Free Segment in the Middle of Span on Structural Behavior.* By analyzing the ratio $\lambda_1$ of the cable-free segment in the middle of the span, the purpose of changing the cable-free segment ratio was achieved by changing the length of the midspan. The length $L_1$ of the cable-free segment in the middle of the span increased from 9.5 mm to 89.5 mm in an amplitude of 10 m. At the same time, the corresponding cable-free segment in the middle of span ratio $\lambda_1$ covered the recommended range of the specification. Finally, through finite element analysis and calculation, the change values of the structural behavior of the structure when the cable-free segment ratio $\lambda_1$ changes were acquired. Figure 9 shows the relationship between the horizontal displacement of the middle pylon and $\lambda_1$; Figure 10 shows the variation of the maximum vertical displacement of the midspan and side span with $\lambda_1$, and Table 1 shows the change of the maximum positive and negative bending moments of the main girder with $\lambda_1$.

It can be seen from Figure 9 that, with the increase of the cable-free segment ratio $\lambda_1$, the horizontal displacement of the middle pylon gradually increases, and the increasing becomes accelerated. The horizontal displacement of the middle pylon increased from 8.17% to 10.37%. By fitting the data, the function expression was acquired as

$$y = 1.34531e^{\lambda_1/0.18614} + 7.54712x + 3.91005. \tag{2}$$

When $\lambda_1 = 0.20$, the horizontal displacement of the bridge pylon is 9.36 mm; when $\lambda_1 = 0.35$, the horizontal displacement of the bridge pylon is 14.24 mm.

It can be seen from Figure 10 that, with the increase of the cable-free segment ratio $\lambda_1$, the deflection of the midspan and the deflection of the side span both increased. The deflection growth trend of the midspan has increased. The increasing ratio of deflection of the midspan increased from 12.24% to 18.28%, and the deflection of the side span increased from 0.08% to 0.06%. It also can be seen that the deflection of the side span remained basically unchanged. The deflection difference between the midspan and the side span also shows an increasing trend of the cable-free segment ratio $\lambda_1$. When the cable-free segment ratio $?_1$ was 0.059, the difference was 19.98 mm, and when $\lambda_1$ was 0.373, the difference was 151.25 mm. The difference shows an exponential growth relationship. Based on the relationship between the deflection of the main girder and the cable-free segment ratio $\lambda_1$, it can be seen that the midspan displacement of the main girder should be paid close attention to when designing the structure.

As shown in Table 1, with the increase of the cable-free segment ratio $\lambda_1$, the maximum positive and negative bending moments of the girder both increased. The maximum positive bending moment of the main girder increased from 44207.6 kN·m to 94948.3 kN·m, an increase of 114.78%, and the maximum negative bending moment increased from 108376.4 kN·m to 186628.8 kN·m, an increase of 72.20%. It can be seen that, with the increase of $\lambda_1$, the rate of increase of the maximum positive bending moment of the main girder is greater than that of the maximum negative bending moment. Since the negative bending moment of the main girder on the top of the pier is much larger than the positive bending moment of the main girder, the abovementioned law can be used to appropriately adjust the ratio $\lambda_1$ of the cable-free segment in the middle of the span to improve the structural force.

*4.2. Influence of Length Variation of the Cable-Free Segment at the Root of Pylon on Structural Behavior.* The same method was used for the analysis of the ratio $\lambda_2$ of the cable-free segment at the root of the pylon. The length $L_2$ of the cable-free segment at the root of the pylon increased from 15.25 m to 55.25 m with an amplitude of 5 m, and the corresponding ratio $\lambda_2$ of the cable-free segment at the root of the pylon covered the recommended range of the specification.

The structural behavior of the structure corresponding to the cable-free segment ratio $\lambda_2$ was calculated by finite element analysis. Figure 11 shows the change of the horizontal displacement of the middle pylon as $\lambda_2$ increasing; Figure 12 shows the change of the maximum deflection of the midspan and the side span as $?_2$ increasing; and Table 2 shows the change of the maximum positive and negative bending moment of the main girder as $\lambda_2$ increasing.

From Figure 11, it can be seen that, with the increase of the cable-free segment ratio $\lambda_2$, the horizontal displacement of the middle pylon gradually increased, and the increasing trend was gradually significant. The horizontal displacement of the middle pylon increased from 6.82% to 10.32%. By fitting the data, the function expression can be acquired as follows:

$$y = 1.32e^{10.19841\lambda_2} + 2.88712. \tag{3}$$

When $\lambda_2 = 0.15$, the horizontal displacement of the bridge pylon was 8.98 mm; when $\lambda_2 = 0.20$, the horizontal displacement of the bridge pylon was 13.04 mm.

It can be seen from Figure 12 that, with the increase of the cable-free segment ratio $\lambda_2$, the deflection of the midspan and the deflection of the side span increase overall. The deflection growth trend of the midspan increased, and the deflection growth trend of the side span first decreased and then increased. The increasing ratio of deflection of the

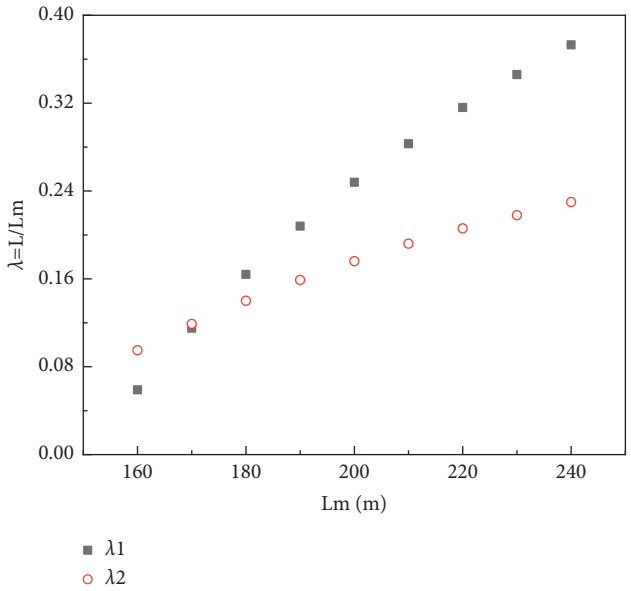


Figure 8: Ratio of cable-free segment and length of the midspan of the girder.

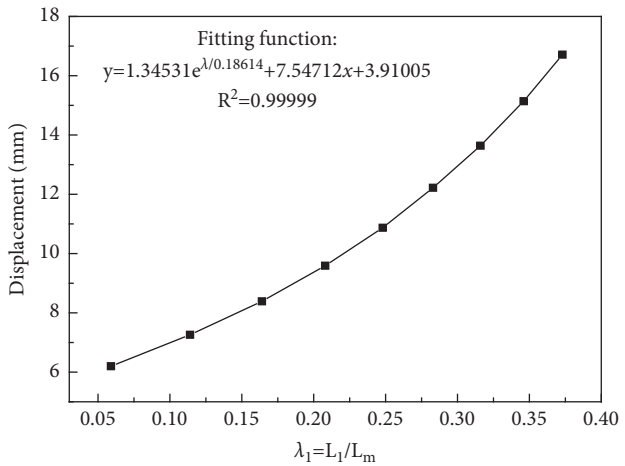


Figure 9: The horizontal displacement of the middle pylon.

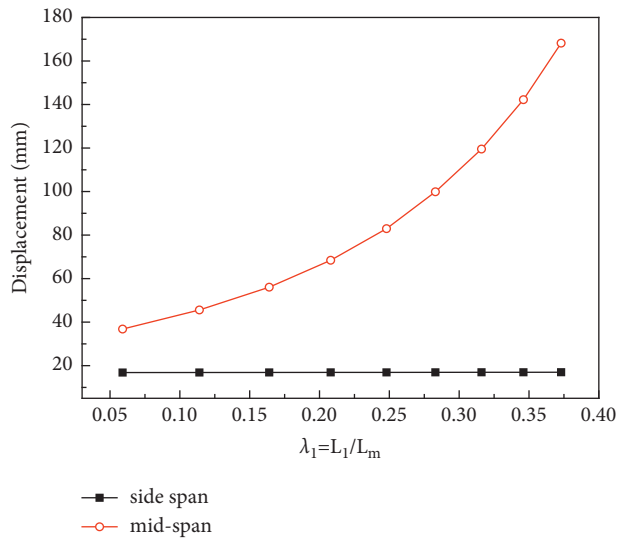


Figure 10: The maximum deflection of the midspan and side span.

Table 1: The maximum positive and negative bending moment of the main girder.

| $\lambda_1 = L_1/L_m$ | Positive bending moment of the girder ($\times 10^3$kN · m) | Negative bending moment of the girder ($\times 10^3$kN · m) |
|---|---|---|
| 0.059 | 44.2076 | 108.3764 |
| 0.114 | 49.3229 | 117.3641 |
| 0.164 | 54.7999 | 126.5615 |
| 0.208 | 60.6307 | 135.9847 |
| 0.248 | 66.8089 | 145.6169 |
| 0.283 | 73.3331 | 155.4684 |
| 0.316 | 80.1993 | 165.5452 |
| 0.346 | 87.4043 | 175.863 |
| 0.373 | 94.9483 | 186.6288 |

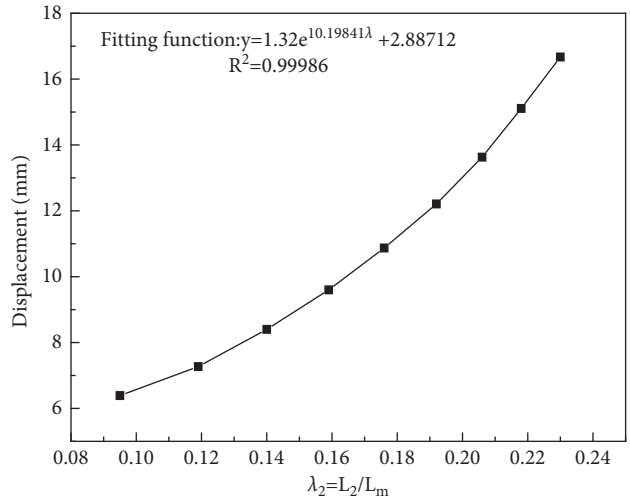


Figure 11: The horizontal displacement of the middle pylon.

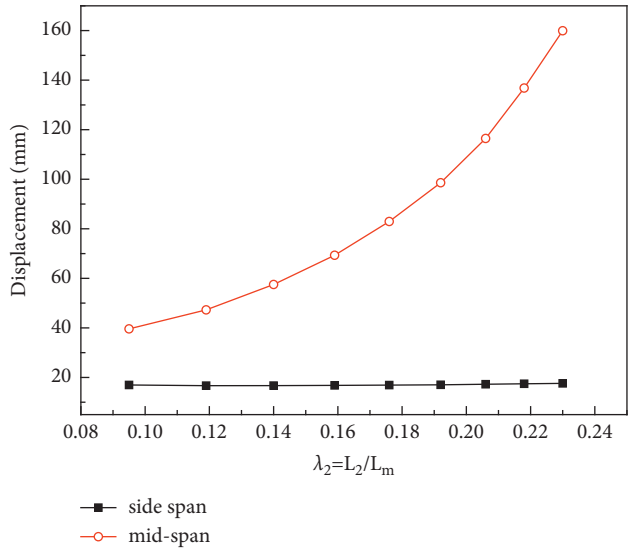


Figure 12: The maximum deflection of the midspan and side spans.

midspan increased from 8.23% to 16.90%, and the deflection of the side span increased from -1.32% to 0.92%. It can be seen that the deflection of the side span only increased by 0.63 mm when $\lambda_2$ increased from 0.095 to 0.230, and the deflection can be considered basically unchanged. The deflection difference between the midspan and the side span of the main girder also showed an increasing trend with the increase of the cable-free segment ratio $\lambda_2$. When the cable-free segment ratio $\lambda_2$ was 0.095, the difference was 22.64 mm, and when $\lambda_2$ was 0.230, the difference was 142.34 mm, and the difference showed an exponential growth relationship. According to the relationship between the deflection of the

Table 2: The maximum positive and negative bending moment of the main girder.

| $\lambda_2 = L_2/L_m$ | Positive bending moment of the girder ($\times 10^3$kN · m) | Negative bending moment of the girder ($\times 10^3$kN · m) |
|---|---|---|
| 0.095 | 48.6167 | 103.9844 |
| 0.119 | 52.3725 | 114.4439 |
| 0.140 | 57.0983 | 124.0347 |
| 0.159 | 61.8727 | 134.4852 |
| 0.176 | 66.8089 | 145.6169 |
| 0.192 | 71.8713 | 157.4713 |
| 0.206 | 77.0726 | 170.0516 |
| 0.218 | 82.425 | 183.3097 |
| 0.230 | 87.9368 | 197.2318 |

girder and the cable-free segment ratio $\lambda_2$, it can be seen that the midspan displacement of the girder should be paid close attention to when designing the structure.

It can be seen from Table 2 that, with the increase of the cable-free segment ratio $\lambda_2$, the maximum positive and negative bending moments of the main girder both increased. The maximum positive moment of the main girder from 48616.7 kN·m increased 87936.8 kN·m, an increase of 80.88%, and the largest negative moment from 103984.4 kN·m increased 197231.8 kN·m, an increase of 89.67%. It can be seen that, with the increase of $\lambda_2$, the increase rate of the maximum negative bending moment of the main girder is greater than the maximum positive bending moment. When the maximum negative bending moment of the main girder was too large, the structure will be unreasonably stressed. Therefore, the ratio $\lambda_2$ of the cable-free segment at the root of the pylon should not be too large in the design.

## 5. Conclusion

In this paper, the influence of length variation of cable-free segment on structural behavior of extradosed bridge was studied. This study explored the relationship between the length of the cable-free segment and the displacement of the bridge pylon, the deflection of the main girder, and the bending moment of the main girder. The following conclusions are drawn:

(1) The accuracy of the finite element software results was verified by comparing the measured data with the theoretical data during the construction stage and after the bridge was completed.

(2) The increase of the ratio $\lambda_1$ of the cable-free segment in the middle of the span magnified the horizontal displacement of the middle pylon. With the increase of the ratio $\lambda_2$ of the cable-free segment at the root of the pylon, the horizontal displacement of the middle pylon increased exponentially.

(3) As the ratio $\lambda_1$ of the cable-free segment in the middle of the span increasing, the positive bending moment of the main girder increased faster than the negative bending moment. With the increase of the ratio $\lambda_2$ of the cable-free segment at the root of the pylon, the increase rate of the negative bending moment of the main girder was greater than the positive bending moment, and the ratio of the cable-free segment at the root of the pylon should be reduced in the design. This rule is proper for using in design.

(4) With the increase in the ratio of the cable-free segment, the deflection of the midspan of the main girder showed an exponential increase, and the deflection of the side span was basically unchanged.

## Data Availability

The data used to support the findings of this study are included within the article.

## Conflicts of Interest

The authors declare that they have no conflicts of interest.

## Acknowledgments

This study was supported by three key funds: the Key Research and Development Program of Heilongjiang Province, China (GZ20210206), and the Fundamental Research Funds for the Central Universities, China (2572020AW53 and 2572019CP02).

## References

[1] R. Xiao, *Bridge Structure System*, China Communications Press, Beijing, 2013.

[2] J. Bujnak, J. Odrobinak, and J. Vican, "Extradosed bridge - theoretical and experimental verification," *Procedia Engineering*, vol. 65, pp. 327–334, 2013.

[3] C. Chen, *Cable-stayed Bridge with Low Pylon*, China Architecture & Building Press, Beijing, 2013.

[4] Q. Pu and H. Zhao, "The effect of side-to-span ratio and cable-free segment length on static and dynamic force of single-pylon cable-stayed bridge," *Journal of Chongqing Jianzhu University*, vol. 32, no. 6, pp. 1101–1105, 2013.

[5] S. Hu, Q. Huang, and Y. Liu, "Validation and numerical calculation of ultimate bending bearing capacity of extradosed bridges," *Journal of South China University of Technology*, vol. 44, no. 8, pp. 114–122, 2016.

[6] B. Peng, D. Yang, and W. Li, "The influence of cable-free segment length on the live load effect of extra-dosed cable-stayed bridge," *Engineering Journal of Wuhan University (Engineering Science Edition)*, vol. 53, no. 4, pp. 324–329, 2020.

[7] W. Liu and Y. Li, "Optimal analysis of the length of extra-dosed bridges," *Journal of China & Foreign Highway*, vol. 30, no. 1, pp. 147–150, 2010.
[8] Z. Zhou and X. Ruan, "The influence of non-cable section of a single-pylon hybrid-girder cable-stayed bridge and its reasonable determination method," *Structural Engineer*, vol. 29, no. 6, pp. 44–48, 2013.
[9] Z. Li, "Sensitivity analysis of the overall design parameters of an extra-dosed bridge," *Journal of China & Foreign Highway*, vol. 34, no. 1, pp. 157–159, 2014.
[10] X. Zhang and Q. Yang, "Study on structural system and static performance of long-span high-pier extra-dosed cable-stayed bridges," *Journal of Zhejiang University of Technology*, vol. 48, no. 1, pp. 112–118, 2020.
[11] C. Luo, X. You, and Y. Zhang, "Study on the influence of the construction error of the super-long-span cable-stayed bridge pylon," *Highway and Transportation Science and Technology*, vol. 26, no. 7, pp. 69–74+79, 2009.
[12] B. Wang and Y.-L. Xu, "Safety analysis of a road vehicle passing by a bridge tower under crosswinds," *Journal of Wind Engineering and Industrial Aerodynamics*, vol. 137, pp. 25–36, 2015.
[13] G. Yan, *Modern Cable-Stayed Bridge*, Southwest Jiaotong University Press, Chengdu, 1996.
[14] L. Jin and H. Guo, "Overview of the development of multi-span cable-stayed bridges," *Highway*, vol. 7, pp. 24–29, 2010.
[15] H. Shi, *Research on Structural System and Parameters of Extra-dosed Cable-Stayed Bridge*, Master thesis of Chang' an University, Xi'an, 2010.
[16] N. Zhang, Y. Liu, J. Liu, D. Ji, J. Fang, and S. F. Stiemer, "Sunshine temperature effect of H-shaped concrete bridge pylon in plateau alpine region," *Journal of Traffic and Transportation Engineering*, vol. 17, no. 4, pp. 66–77, 2017.
[17] Z. Liu, J. Xin, S. Zhou, and F. Bao, "Sensitivity analysis of parameters of cable-stayed bridges with special-shaped pylons," *Journal of China & Foreign Highway*, vol. 40, no. 5, pp. 76–80, 2020.
[18] D. Sun and G. Zhang, "Length parameters effect analysis of the single-cable-stayed extra-dosed bridge," *Structural Engineers*, vol. 09, no. 1, pp. 33–39, 2013.
[19] Y. Jiang, G. Yang, and H. Song, "Dynamic optimization design of extra-dosed cable-stayed bridge under earthquake excitation," *Engineering Mechanics*, vol. 37, pp. 313–319, 2020.
[20] F. Wang and H. Yuan, *Specifications for Design of Highway Cable-stayed Bridge*, China Communications Press, Beijing, 2020.
[21] L. S. Hsu and C.-T. T. Hsu, "Complete stress - strain behaviour of high-strength concrete under compression," *Magazine of Concrete Research*, vol. 46, no. 169, pp. 301–312, 1994.
[22] W. Han and Y. Lu, "Experimental research on prediction model of concrete shrinkage and creep," *Journal of Central South University*, vol. 47, no. 10, pp. 3515–3522, 2016.